

Comparative Analysis to Predict the Temperature Rise in 3ϕ -Squirrel Cage Induction Motor using Lumped Parameter Thermal Model and Finite Element Method for Industrial Applications

S. Sachin^{1*}, Krishnan Manickavasagam² and A. T. Sriram³

¹Department of Electrical Engineering, M. S. Ramaiah University of Applied Sciences, Bengaluru 560054, Karnataka, India; sachins.schms@gmail.com

²Department of Electrical and Electronics Engineering Education National Institute of Technical Teachers Training and Research, Bhopal - 462 002, Madhya Pradesh, India; kmanickavasagam@nitttrbpl.ac.in

³Department of Automotive and Aeronautical Engineering, M. S. Ramaiah University of Applied Sciences, Bengaluru 560054, Karnataka, India; atsriram.aae.et@msruas.ac.in

Abstract

The 3ϕ - Squirrel Cage Induction Motor (SCIM) used in industrial are prone to thermal breakdown due to its working conditions. Losses in the motor cause rise in temperature. Losses estimation of the 3ϕ - SCIM play a very important role in analyzing the electrical and thermal performances. In this paper a Lumped Parameter Thermal Model (LPTM) and Finite Element Method (FEM) is used to estimate the temperature rise in 3ϕ - SCIM. The temperature rise is obtained considering loss, with load variation between no-load to full load conditions, this enables to analyse the application of induction motor in mines. In addition to that a comparative analysis is carried out between Lumped Parameter Thermal Model (LPTM) and Finite Element Method (FEM) to determine the effective method to estimate temperature rise and determine the relative percentage error in temperature rise at various elements of 3ϕ - SCIM.

Keywords: Finite Element Method (FEM), Lumped Parameter Thermal Model (LPTM), Squirrel Cage Induction Motor (SCIM).

1.0 Introduction

The demand for effective operation of induction motor has become necessary in industrial, domestic, manufacturing, excavation, mines and many other applications. The SCIM meet all necessities of small - large scale industries. The inner parts of SCIM are stator and rotor. The main problem in is rise in temperature in its parts. When SCIM is working continuously, the temperature rise may cross the thermal

limit, leading to failure. The failure in stator and rotor of SCIM is more than 70%¹. Rotor bars and stator conductors will collapse due to high temperature rise. Temperature rise of SCIM becomes a primary technical challenge in design of SCIM. In design process it is essential to know the temperature rise in major part of SCIM².

SCIM's are typical used in industrial applications, because of its rugged construction and low cost. One of the major reason for temperature rise is loss dissipation.

*Author for correspondence

The loss dissipation in SCIM increases the temperature in various parts, viz. stator windings, rotor bars, and motor outer frame etc. The heat generated in SCIM can be extracted via conduction, convection and radiation³. The SCIM can be protected from high temperature rise, by reducing losses and by providing cooling system⁴.

Thermal analysis of SCIM is more important compared to Electro-Magnetic Analysis (EMA) as it is dependent on material properties and on the manufacturing⁵. The heat contribution of rotor in SCIM is 5% from rotor iron losses and 15% from rotor copper loss, 20% from stator iron loss, 40% from stator copper loss, mechanical losses and stray losses contributes 20%⁶⁻⁹.

The temperature rise in SCIM may increases, due to overloaded condition, inadequate ventilation and high ambient working temperatures. The temperature rise may damage the insulation in the stator windings, rotor bars and insulation between laminations¹⁰⁻¹⁴. In order to analyse the temperature rise in various parts of the SCIM, thermal analysis is carried out using LPTM and FEM method. The thermal analysis of SCIM dependent on material used in different parts, area of application, operating condition and ambient temperature¹⁵⁻²⁰.

In this study, the temperature rise measurement is performed using a 15 kW, 3-SCIM. A 3D FEM and LPTM model of the 3Φ-SCIM is created, and the temperature rise is examined under various load conditions at a 25°C room temperature. The work flow of the paper is as in Figure 1.

The objective of the paper is:

- Estimation of temperature rise with respect to LPTM
- Estimation of temperature rise with respect to 3D – FEM
- Carryout comparative analysis between LPTM and 3D – FEM model and calculate relative % error.

2.0 Loss Estimation of 3Φ - SCIM

Conventionally, factors observed while operation of SCIM have been used to determine copper losses. Copper loss calculations are based on current drawn.

The equations used to evaluate the losses are as follows:

The input power of the stator:

$$P_1 = \sqrt{3} * V_{line} * I_{line} * \cos\phi \tag{1}$$

The magnetization current is neglected. $I_1 = I_2'$ (2)

The synchronous speed is given by: $N_s = \frac{120 * f}{p}$,

$$\omega_s = \frac{2 * \pi * N_s}{60} \tag{3}$$

The Slip $N = (1 - S)N_s$ (4)

The copper loss at stator is given by:

$$P_{cu} = 3 * (I_L)^2 * R_s \tag{5}$$

The input power at rotor is estimated using:

$$P_2 = \omega_s * T \tag{6}$$

The Al losses at rotor is estimated using:

$$P_{Al} = 3 * I_2'^2 * r_2' = S * P_2 \tag{7}$$

Mechanical power developed is given by

$$P_m = (1 - S) * P_2 \tag{8}$$

Losses (Mechanical) $P_m = P_0 + \text{Mechanical losses}$ (9)

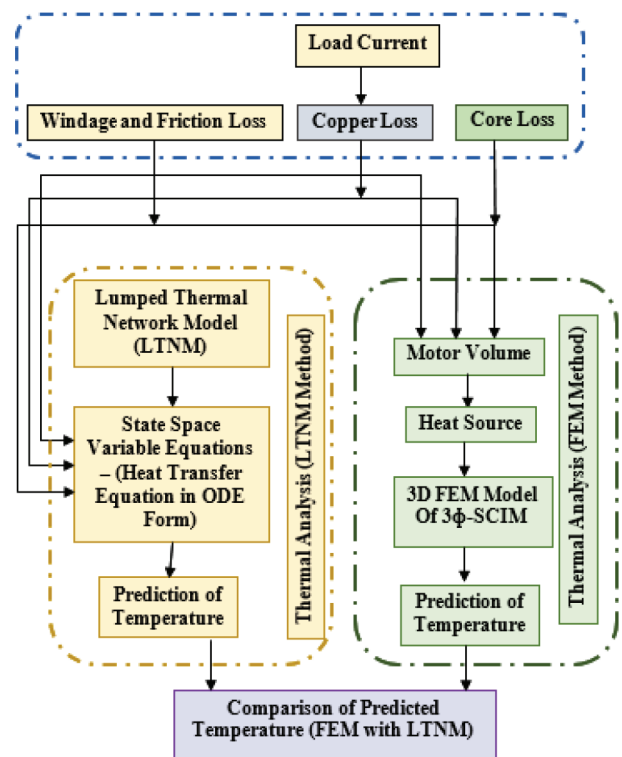


Figure 1: Block diagram of proposed method.

The total core losses is estimated by:

$$P_1 = P_2 + P_{cu} + P_{iron} + \text{Additional losses} \quad (10)$$

At all the load conditions core loss is assumed constant. Table 1 contains the SCIM's specs. The calculated losses of 15kW 3ϕ - SCIM at full load condition is listed in Table 2.

3.0 Thermal Analysis-Lumped Parameter Thermal Model (LPTM)

The temperature of SCIM is predicted using LPTM, and is made up of thermal resistance, capacitance and the heat sources. The conductive resistance is calculated using the geometry and material characteristics. The convective thermal resistance is estimated using the Prandtl and Reynolds values. In this case, the effect of radiation is neglected. Calculated thermal resistance, heat sources, and heat movement at each node is the foundation of the

Table 1: Specification of 15kW 3ϕ - SCIM

Parameters	Parameters 15kW SCIM
Rated Supply Voltage	415 V
Rated line current	28.18 A
Current at no-load	11.72 A
Rated power	15 kW
Number of pole	4
Rated speed of motor	1462 RPM
Motor speed at no-load	1488 RPM
Motor efficiency	90%
Torque	97.98 N-m
Ambient temperature	25 °C

Table 2: Losses in 15 kW 3ϕ - SCIM

Loss Label	Losses (W)
Friction and windage losses	83.4
Iron losses	310.5
Stator copper losses	654.2
Rotor aluminum losses	409.7
Additional losses	199.9
Losses at rated load	1658
Losses at no-load	517

LPTM. Temperature varies with respect to time and is as given by ODE equation (11).

$$pC_p V \frac{dT}{dt} = Q_{in} - Q_{out} + Q_{generated} \quad (11)$$

The LPTM has included the heat transfer mechanisms and main elements within the 3ϕ-SCIM. The SCIM is split into lumped elements, having thermal storage and heat generation, interconnecting with nearby components.

The 15kW, 3ϕ-SCIM is divided into main ten components and is shown in Figure 2, the SCIM is symmetrical on its axis.

Since all components are cylindrical, the thermal resistances are now determined using cylindrical lumped components. The convective heat transfer technique is used to determine the thermal resistances of the air gap and end cap air. As shown in Figure 3, the network of ten

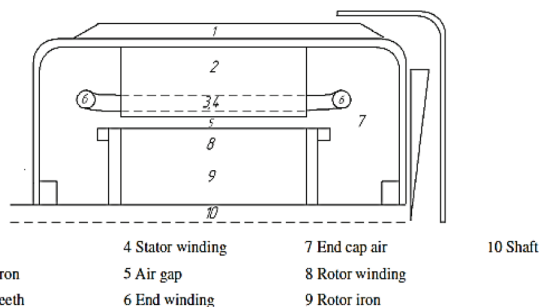


Figure 2: Ten elements considered to develop LPTNM⁴.

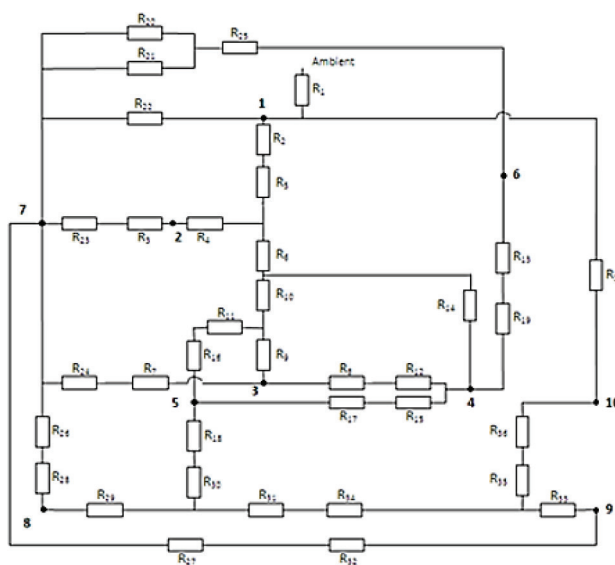


Figure 3: Ten Element LPTM of SCIM⁴.

elements represents the total ten element LPTM of the 15kW, 3Φ-SCIM.

From the energy balance equation (11), mathematical formulae that describe the thermal behavior of 3Φ-SCIM are obtained.

3.1 Performance of LPTM

In this session, the performance of the 10-element LPTM of the 3Φ-SCIM is used to evaluate the temperature rise at various nodes using equation (12).

$$dT = A * T + u * B \tag{12}$$

where, 'A' is a conductance matrix, 'B' is a loss matrix, and 'u' is an unity matrix.

The losses in SCIM determines the temperature rise at various load conditions. The estimated temperature rises at various parts of SCIM, at different load conditions considering losses is as presented in Table 3.

The results presented in Table 3 is for major 4 elements (Stator Winding (SW), Stator Core (SC), Rotor Core (RC) and Rotor Winding (RW)) for which the comparison is carried out with FEM analysis (Sachin S. 2022)

3.2 Thermal Analysis – 3D Fem Model

The rise in temperature in 3Φ-SCIM is because of the motor losses. In this research, the variation in temperature is accounted for the loss assessment. A 3D FEM model is developed for evaluation of rise in temperature at various parts of the 3Φ-SCIM at different load conditions

The 3D model is meshed using the HYPERMESH tool, as seen in Figure 4. Figure 5 illustrates how the generated meshed 3D model looks in the CFD tool, and evaluates the rise in temperature at various part of the SCIM as show in Figure 6. The losses per volume fed to the 3D CFD model and enumerated in Table 4 are used to determine heat sources in SCIM.

The rise in temperature in 3Φ-SCIM is analyzed using the computational tool ANSYS CFX. Table 4 lists the heat sources that were determined for the 15 kW 3Φ-SCIM. In order to predict the increase in temperature, the 3D-CFD model incorporates the predicted heat sources.

For the 15 kW 3Φ-SCIM, the temperature increase is calculated at 25⁰C ambient temperature as shown in Figure 6. The rise in temperature at different load conditions is observed. The temperature rises is maximum at Stator Windings (SW), Stator Core (SC), Rotor Windings

Table 3: Rise in temperature at various parts of 3Φ-SCIM - LPTM

Element / Load	Considering Constant Core Loss			
	No-Load	Half Load	3/4th load	Full Load
Stator Core	24.36	28.11	61.95	95.05
Stator Winding	23.29	27.18	61.36	94.77
Rotor Winding	21.41	25.41	58.70	91.28
Rotor Core	20.98	24.93	57.97	90.31

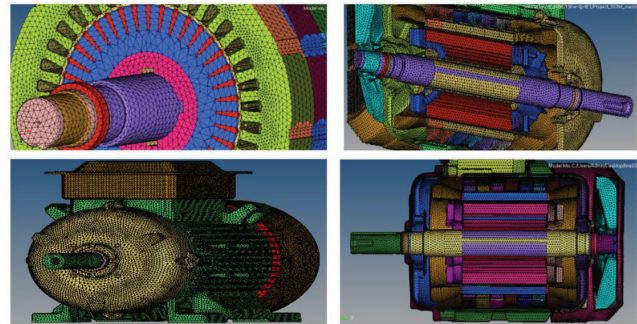


Figure 4: Cross section view of overall 2D meshed model with common surface.

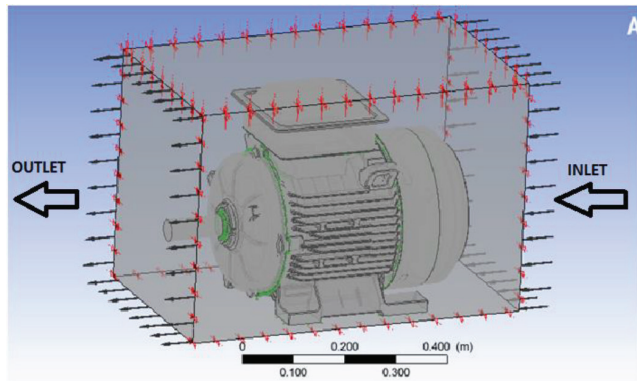


Figure 5. Overall CFX model setup file.

Table 4: Heat sources of 15 kW SCIM at different loads

Motor Component	No Load	Half Load	3/4th Load	Full Load
	δ in W/ m ³			
Stator conductors	41860	63178	173643	250000
Stator core	56795	56795	56795	56795
Rotor core	71148	71148	71148	71148
Rotor bars (each)	462	4759	7388	9629

(RW), and Rotor Core (RC). Figure 7 depicts the rise in temperature at different parts of SCIM. Figure 8 depicts the distribution of temperature as seen in flat part of the SCIM (Sachin S. 2022).

3.3 Temperature Rise in SCIM

The temperature rise at various part of the 15 -kW 3 ϕ -SCIM are as given in Table 5 and is as shown in Figure 8.

3.4 Comparative Analysis

The estimated temperature considering LPTM and FEM in Stator Winding (SW), Stator Core (SC), Rotor Core (RC) and Rotor Winding (RW) is as plotted in Figure 9, Figure 10, Figure 11 and Figure 12 respectively.

In all the plots X-axis is Load and Y-axis is temperature rise. The plots of Load vs. temperature rise it is evident that the FEM analysis is yielding more reliable results. LPTM uses Ordinary Differential Equations (ODE) and is solved using state space variable technique. LPTM is

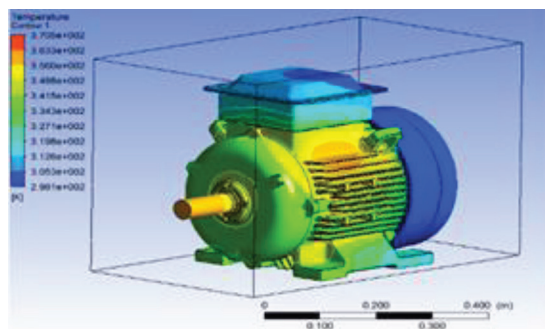


Figure 6: Overall temperature distribution in 15 kW SCIM.

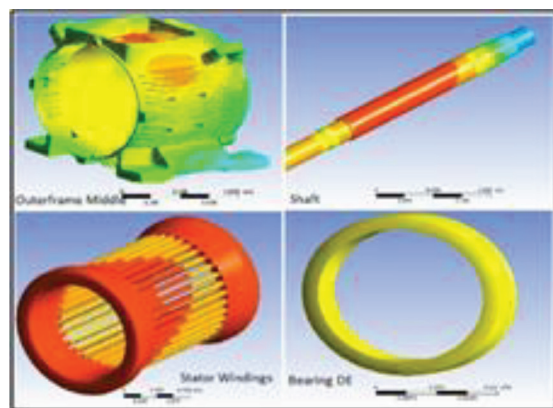


Figure 7: Temperature at various parts of motor.

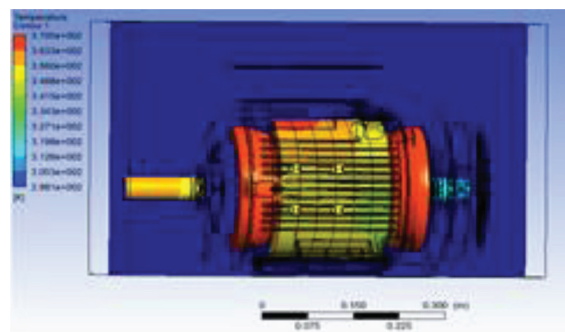


Figure 8: Temperature distribution in plane section of the motor.

Table 5: Rise in temperature at various parts of 3 ϕ -SCIM – 3D-FEM model

Motor Component	Rise in Temperature ($^{\circ}$ C)			
	No Load	Half Load	$\frac{3}{4}$ th Load	Full load
Stator Winding (SW)	29.55	35.31	51.15	68.15
Stator Core (SC)	23.57	30.08	44.23	58.46
Rotor Core (RC)	27.17	34.63	49.52	65.74
Rotor Windings (RW)	26.87	34.28	49.64	65.36

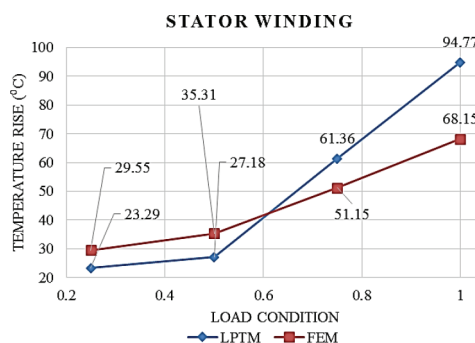


Figure 9: Stator winding temperature rise.

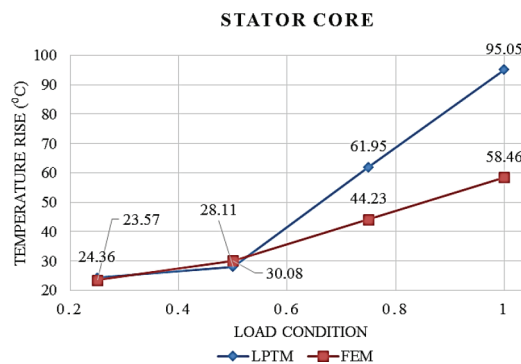


Figure 10: Stator core temperature rise.

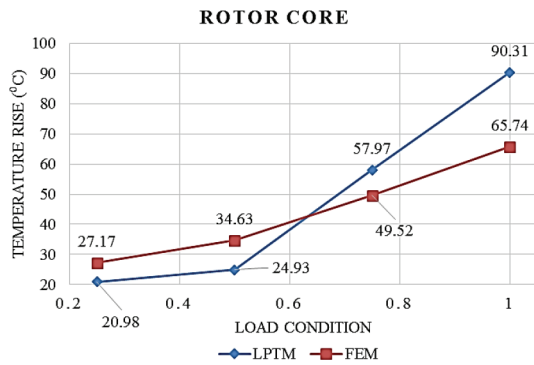


Figure 11: Rotor core temperature rise.

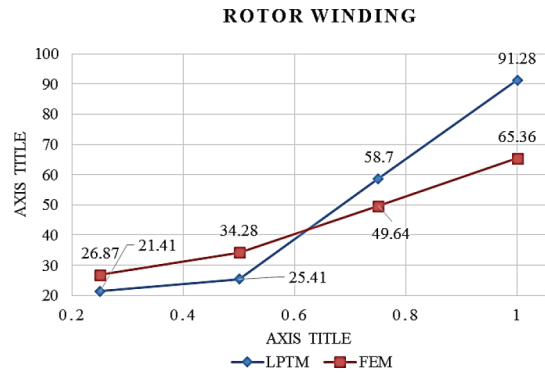


Figure 12: Rotor winding temperature rise.

Table 6: Relative %error between LPTM and FEM

Load Condition	Temperature Rise (°C)			
	No-Load	Half Load	3/4th Load	Full Load
SW- LPTM	23.29	27.18	61.36	94.77
SW- FEM	29.55	35.31	51.15	68.15
% error	21.18	23.02	-19.96	-39.06
SC- LPTM	24.36	28.11	61.95	95.05
SC- FEM	23.57	30.08	44.23	58.46
% error	-3.35	6.55	-40.06	-62.59
RC- LPTM	20.98	24.93	57.97	90.31
RC- FEM	27.17	34.63	49.52	65.74
% error	22.78	28.01	-17.06	-37.37
RW- LPTM	21.41	25.41	58.7	91.28
RW- FEM	26.87	34.28	49.64	65.36
% error	20.32	25.88	-18.25	-39.66

a 1D system comprising of thermal resistances, which is only dependent on material and geometry of the SCIM. LPTM is a linear system as it used ODE.

FEM analysis uses Partial Differential Equations (PDE), and is nonlinear system. PDE's are solved using numerical techniques with convergence accuracy of 1×10^{-4} . Hence the results of FEM analysis is more reliable than LPTM. ANSYS Maxwell tool is used to carry out FEM analysis. MATLAB is used to carry out LPTM analysis. The relative % error between LPTM and FEM analysis and is as tabulated in Table 6.

4.0 Conclusion

A LPTM and FEM is constructed for the thermal analysis of 15kW 3Φ-SCIM. The motor's steady-state temperature can be determined analytically using the LPTM model at

the early stages of construction or design. Most 3Φ-SCIM can be simply fitted with the model. However, due to many simplifications, the LPTM model's accuracy is limited. LPTM is designed for 15kW 3Φ-SCIM in this case and temperature rise is obtained at various load conditions. Similarly, 3D model is developed for 15kW 3Φ-SCIM and thermal analysis is carried out using FEM with convergence accuracy of 1×10^{-4} . Results of temperature rise at Stator Winding (SW), Stator Core (SC), Rotor Core (RC), and Rotor Winding (RW) are plotted. Relative % error is calculated. Analysis concluded that FEM analysis yields better and reliable results than LPTM.

5.0 References

1. Bousbaine A. An investigation into the thermal modelling of induction motors (Doctoral dissertation, University of Sheffield).

2. Kylander G. Thermal modelling of small cage induction motors. Chalmers Tekniska Hogskola (Sweden); 1995.
3. Liang D, Zhu ZQ, Feng JH, Guo SY, Li YF, Wu JQ, Zhao AF. Influence of critical parameters in lumped-parameter thermal models for electrical machines. 22nd International Conference on Electrical Machines and Systems (ICEMS); 2019 Aug 11-14; China: Harbin; 2019. p. 1-6. <https://doi.org/10.1109/ICEMS.2019.8921846>
4. Mellor PH, Roberts D, Turner DR. Lumped parameter thermal model for electrical machines of TEFC design. IEE Proceedings B (Electric Power Applications). 1991; 138(5):205-18. <https://doi.org/10.1049/ip-b.1991.0025>
5. Popova L, Nerg J, Pyrhönen J. Combined electromagnetic and thermal design platform for totally enclosed induction machines. 8th IEEE Symposium on Diagnostics for Electrical Machines, Power Electronics and Drives; 2011 Sep -8; Italy: Bologna; 2011. p. 153-8. <https://doi.org/10.1109/DEMPED.2011.6063617>
6. Sachin S, Sriram AT. Review of physical and mathematical modelling aspects of thermal management of induction motors. Journal of Physics: Conference Series; 2020; 1706(1). <https://doi.org/10.1088/1742-6596/1706/1/012105>
7. Hooli S, Vadde A, Manickavasagam K, Kadambi GR. Measurement of torque using leakage flux for induction motors in electric vehicles by non-invasive method. Innovations in Electrical and Electronic Engineering: Proceedings of ICEEE 2020; 2021. p. 489-503. https://doi.org/10.1007/978-981-15-4692-1_38
8. Khazi S, Vadde A, Manickavasagam K, Kadambi GR, Narayanan V, Lokesh BM, *et al.* Analyzation of temperature rise in induction motor for electric vehicles. Advances in Energy Technology: Select Proceedings of EMSME 2020; 2022. p. 173-83. https://doi.org/10.1007/978-981-16-1476-7_17
9. Hooli SS, Vadde A, Manickavasagam K, Kadambi GR. Fuzzy based health monitoring of electric vehicle motor using time domain analysis. 2021 International Conference on Sustainable Energy and Future Electric Transportation (SEFET); 2021 Jan 21-23; India: Hyderabad; 2021. p. 1-6. <https://doi.org/10.1109/SeFet48154.2021.9375791>
10. Boglietti A, Cavagnino A, Staton DA, Popescu M, Cossar C, McGilp MI. End space heat transfer coefficient determination for different induction motor enclosure types. 2008 IEEE Industry Applications Society Annual Meeting; 2008 Oct -9; Canada: Edmonton, AB; 2008. p. 1-8. <https://doi.org/10.1109/08IAS.2008.49>
11. Boglietti A, Cavagnino A, Staton D, Shanel M, Mueller M, Mejuto C. Evolution and modern approaches for thermal analysis of electrical machines. IEEE Transactions on Industrial Electronics. 2009; 56(3):871-82. <https://doi.org/10.1109/TIE.2008.2011622>
12. Dutta B, Chowdhury SK. Steady state thermal model of TEFC induction machine. 2012 IEEE International Conference on Power Electronics, Drives and Energy Systems (PEDES); 2012 Dec 16-19. India: Bengaluru; 2012. p. 1-6. <https://doi.org/10.1109/PEDES.2012.6484344> PMCid:PMC3417975
13. Gao Z. Sensorless stator winding temperature estimation for induction machines. Conference Record of the 2006 IEEE Industry Applications Conference Forty-First IAS Annual Meeting; 2006 Oct 8-12. USA: Tampa, FL; 2006. <https://doi.org/10.1109/IAS.2006.256559>
14. Gao Z, Habetler TG, Harley RG, Colby RS. An adaptive Kalman filtering approach to induction machine stator winding temperature estimation based on a hybrid thermal model. Fourtieth IAS Annual Meeting. Conference Record of the 2005 Industry Applications Conference; 2005.
15. Mynarek P, Kowol M. Thermal analysis of three-phase induction motor using circuit models. Electrodynamic and Mechatronic Systems; 2011. p. 119-122. <https://doi.org/10.1109/SCE.2011.6092137>
16. Staton D, Boglietti A, Cavagnino A. Solving the more difficult aspects of electric motor thermal analysis in small and medium size industrial induction motors. IEEE Trans Energy Convers. 2005; 20(3):620-8. <https://doi.org/10.1109/TEC.2005.847979>
17. Sachin S, Manickavasagam K, Sriram AT. Effect of the temperature fluctuation on torque production by assimilating variable core loss using computational approach for electric vehicles motors. Int Rev Electr Eng. 2022; 17(6). <https://doi.org/10.15866/iree.v17i6.22503>
18. Sachin S, Manickavasagam K, Sriram AT. Effect of core losses on thermal analysis of 3 Φ -Squirrel Cage Induction Motor using lumped parameter thermal model. Mater Today Proc. 2023; 80:724-30. <https://doi.org/10.1016/j.matpr.2022.11.076>
19. Sudha B, Vadde A, Manickavasagam K. Thermal behavior on Productive torque in electric vehicle motor using computational methods. 2021 IEEE 6th International Conference on Computing, Communication and Automation (ICCCA); 2021. p. 367-71.
20. Sudha B, Vadde A, Manickavasagam K, Kadambi GR. Characterization of temperature and productive torque for 160L frame Squirrel Cage Induction Motor. J Eng Res. 2021. p. 35-46.